Classical momentum distributions of Rydberg states

Inés Samengo
Centro Atómico Bariloche and Instituto Balseiro, 8400 San Carlos de Bariloche, Río Negro, Argentina
(Received 16 April 1998)

We give exact analytical expressions for the classical distributions corresponding to the momentum representation of Rydberg states. [S1050-2947(98)00610-6]

PACS number(s): 31.15.−p, 31.15.Gy, 03.65.Sq

I. INTRODUCTION

Almost all of what we currently know about microscopic phenomena is due to the revolutionary results of quantum mechanics, early in this century. At the present time, nearly a hundred years later, experiments are being made on the very border of microscopic and macroscopic systems. It is now possible to accommodate atomic electrons in highly excited Rydberg states, with fine control of their orientation and aligment [1–5]. As stated in Ref. [6], in these systems the size of an atom is a good measure of the validity of classical mechanics. Currently, experimentalists can excite atoms and make them as big as bacteria. The evolution of such systems could be described, in principle, by quantum mechanics. However, the huge calculations involved make the problem untreatable. In consequence, for practical reasons researchers have begun to turn back to classical physics.

For most macroscopic systems classical methods give a good description of the experimental results. This is why classical trajectory Monte Carlo calculations have been so widely used (for examples in Rydberg states, see Refs. [7–11]). However, on the very border of the validity of classical physics, some of the statistical properties of matter have to be retained. In classical descriptions, this is usually done by averaging over many realizations with a weight function given by the initial state, which is taken to be a quantum-mechanical distribution. This approach, although successful in many cases, is not entirely consistent with the whole theory, since it is known that the square modulus of a stationary wave function is not necessarily stationary under the action of the classical evolution operator. There is therefore a consistency reason for studying classical distributions corresponding to quantum-mechanical stationary states.

Finally, classical physics has some very elegant aspects, such as its simple scaling laws, and its transparent causality. These features provide, in addition to their own beauty, an interesting insight into the corresponding quantum-mechanical processes.

Following this *renaissance* of the old approach to atomic physics, in this paper we calculate the classical distribution of particles corresponding to the quantum-mechanical Rydberg states. We use the expression *Rydberg state* to designate the stationary wave functions of the Coulomb potential, characterized by definite values of the energy, the square modulus of the angular momentum, and one of its components. We proceed in the following way. We construct an ensemble of classical trajectories which correspond to Rydberg states. We select the orbits which have the same values of E, L^2, and L_z as the corresponding wave functions. Each of the trajectories that belongs to the ensemble contributes to the total particle distribution with a characteristic density. We construct the classical Rydberg distributions summing up all these individual densities.

It is known that in the Coulomb potential there is a coordinate transformation which maps Kepler ellipses into uniform circular motion. Clearly, uniform motion gives the simplest possible particle distribution, namely, a uniform distribution on each orbit. We shall exploit this simplicity when constructing our classical Rydberg states. In Sec. II we characterize the motion in the new coordinates, called symmetric variables. In Sec. III we use these coordinates to construct the classical Rydberg momentum distributions, which are the main result of this paper. After that, in Sec. IV we present an example in coordinate space. We end in Sec. V with some concluding remarks.

II. THE KEPLER TRAJECTORIES

In this section we review the classical description of the Coulomb potential, both in real and symmetric space. We follow the approach presented by Györgyi in Ref. [12].

We consider a particle of mass m in the potential

$$V(\mathbf{r}) = -\frac{g}{r}.$$

The position of the particle is given by the vector $\mathbf{r} = r\hat{r} = r_1\hat{y} + r_2\hat{x} + r_3\hat{z}$, where the symbol $\hat{r}$ represents a unit vector in the direction of $\mathbf{r}$. Using $\mathbf{p} = p\hat{p} = p_1\hat{p}_y + p_2\hat{p}_x + p_3\hat{p}_z$ for the momentum, the Hamiltonian of the system reads

$$\mathcal{H}(\mathbf{r},\mathbf{p}) = \frac{p^2}{2m} - \frac{g}{r}.$$

Since the Hamiltonian is a conserved quantity, we can write its numerical value as

$$\mathcal{H} = E = -\frac{p_E^2}{2m} = -\frac{g}{2r_E} = -\frac{g^2 m}{2L_E^2},$$

where E, p_E, r_E, and L_E are constants which parametrize the energy, with units of energy, momentum, position, and angular momentum, respectively.

The evolution of the particle is governed by Hamilton equations, namely,

$$\frac{dr_i}{dt}=\frac{\partial \mathcal{H}}{\partial p_i}, \quad \frac{dp_i}{dt}=-\frac{\partial \mathcal{H}}{\partial r_i}, \tag{1}$$

where the subindex i runs from 1 to 3.

Instead of trying to solve these equations explicitly, we introduce the vectors

$$\mathbf{L}=\mathbf{r}\times\mathbf{p}, \quad \text{angular momentum},$$

$$\mathbf{A}=r_E p_E \frac{\mathbf{r}}{r}-\frac{\mathbf{p}}{p_E}\times\mathbf{L}, \quad \text{Runge-Lenz vector}.$$

With this definition, both vectors have the same units. Each of their components is a constant of motion, as may be seen by explicitly calculating their Poisson brackets with the Hamiltonian. We therefore have seven conserved quantities: $\mathcal{H}$, L_1, L_2, L_3, A_1, A_2, and A_3. They are functions of the coordinates **r** and **p**. The trajectory of the particle has to be contained in the surfaces defined by the values of these quantities.

Phase space has dimension six. As each conserved quantity defines a surface of dimension five, and a trajectory has dimension one, it is not possible to have more than five independent constants of motion. In fact, the seven conserved quantities obey the relations

$$0=\mathbf{L}\cdot\mathbf{A}, \tag{2}$$

$$L_E^2=A^2+L^2, \tag{3}$$

as may be checked from their very definition. Equation (2) restricts the angle between **L** and **A**, imposing orthogonality. Equation (3) is a relation between their moduli.

We define the angle

$$\alpha_0=\arctan(L/A).$$

Once the energy is given, fixing α_0 determines L and A, namely,

$$L=L_E \sin\alpha_0, \quad A=L_E \cos\alpha_0,$$

with α_0 in $[0,\pi/2]$.

We aim at obtaining the stationary particle distribution for a specific ensemble of Kepler orbits. Therefore we are not interested in the time evolution of individual particles. Instead of attempting to solve Hamilton equations (1), we search for the geometrical locus of the trajectories. This we do with the help of the conserved quantities.

A. Coordinate and momentum spaces

Let us begin with coordinate space. By simple calculation, the following relations can be verified:

$$0=\mathbf{L}\cdot\left(\mathbf{r}-r_E\frac{\mathbf{A}}{L_E}\right), \tag{4}$$

$$\mathbf{0}=\mathbf{A}\times\left(\mathbf{r}-r_E\frac{\mathbf{A}}{L_E}\right)-\sqrt{r_E^2-\left|\mathbf{r}-r_E\frac{\mathbf{A}}{L_E}\right|^2}\,\mathbf{L}. \tag{5}$$

Equation (4) confines the trajectory to the plane perpendicular to the angular momentum. Equation (5), when restricted to this plane, defines an ellipse, shown in Fig. 1(a). The parameter r_E constitutes a scale factor for the orbit.

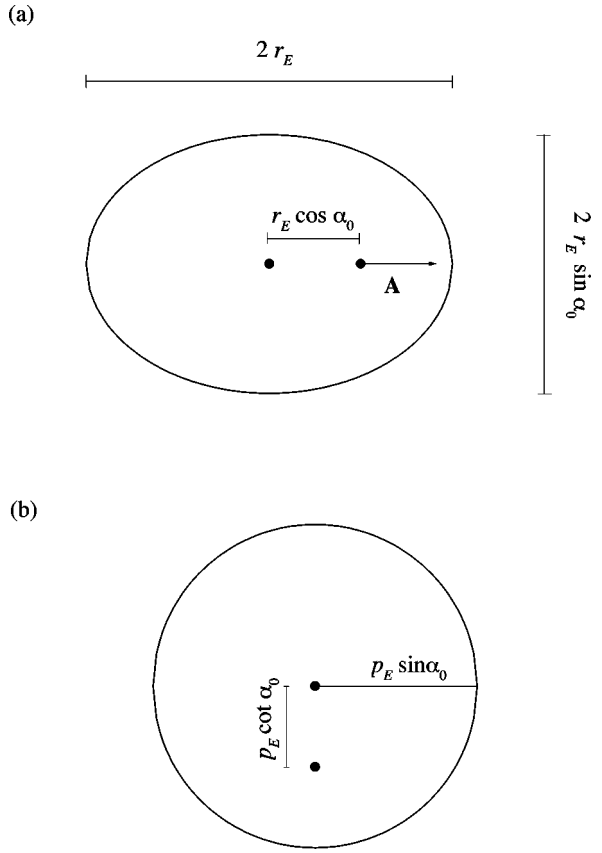

FIG. 1. (a) Trajectory of the particle in coordinate space for $\alpha_0=60°$. The major axis of the ellipse is oriented in the direction of **A** and has a length of $2r_E$. The minor axis points towards $\mathbf{L}\times\mathbf{A}$, and is $2r_E\sin\alpha_0$ long. The eccentricity is $\epsilon=\cos\alpha_0$. The geometrical center of the ellipse is displaced from the force center in the direction of $-\mathbf{A}$, a distance $r_E\cos\alpha_0$. (b) Trajectory of the particle in momentum space for $\alpha_0=60°$. The circle has a radius $p_E/\sin\alpha_0$, and its center is displaced from the origin in the direction $\hat{L}\times\hat{A}$, a distance $p_E\cot\alpha_0$.

The equations for the trajectory (4) and (5) are a set of four nonhomogeneous nonlinear relations for the components of the position vector **r**. Since **L** and **A** are orthogonal, only two of them, Eqs. (4) and (5), are independent. These two scalar equations define a curve in coordinate space.

We now analyze the trajectories in momentum space. Once more, the following relations can be explicitly verified:

$$0=\mathbf{L}\cdot\mathbf{p}, \tag{6}$$

$$\mathbf{0}=\mathbf{A}\times\mathbf{p}-\frac{p_E^2-p^2}{2p_E}\mathbf{L}. \tag{7}$$

Equation (6) confines the trajectory to the plane perpendicular to the angular momentum. Equation (7), when restricted to this plane, defines a circle. We depict it in Fig. 1(b). The

scale factor of the orbit is now p_E. Once more, we have that only two of the four scalar equations (6) and (7) are independent.

B. The symmetric representation

We now want to make explicit use of the hidden symmetry of the Coulomb problem, in order to map Kepler orbits to uniform circular motion. Following Fock [13], we introduce the variables

$$\begin{aligned}
\rho_1 &= r_1 - r_E\frac{A_1}{L_E}, \quad \pi_1 = \frac{2p_E^2}{p_E^2+p^2}p_1,\\
\rho_2 &= r_2 - r_E\frac{A_2}{L_E}, \quad \pi_2 = \frac{2p_E^2}{p_E^2+p^2}p_2,\\
\rho_3 &= r_3 - r_E\frac{A_3}{L_E}, \quad \pi_3 = \frac{2p_E^2}{p_E^2+p^2}p_3,\\
\rho_4 &= \sqrt{r_E^2 - \left|\mathbf{r} - r_E\frac{\mathbf{A}}{L_E}\right|^2}, \quad \pi_4 = \frac{p_E^2-p^2}{p_E^2+p^2}p_E,
\end{aligned} \tag{8}$$

which we call symmetric coordinates. The spatial coordinate $\mathbf{r}$ along with r_E are transformed into the four-dimensional vector $\vec{\rho}=(\rho_1,\rho_1,\rho_3,\rho_4)$. The momentum $\mathbf{p}$, together with p_E, are mapped into $\vec{\pi}=(\pi_1,\pi_2,\pi_3,\pi_4)$. It can be verified that

$$\begin{aligned}
|\vec{\rho}|^2 &= \rho_1^2+\rho_2^2+\rho_3^2+\rho_4^2 = r_E^2,\\
|\vec{\pi}|^2 &= \pi_1^2+\pi_2^2+\pi_3^2+\pi_4^2 = p_E^2.
\end{aligned} \tag{9}$$

Equations (9) show that the transformation (8) maps the whole of three-dimensional coordinate (momentum) space, onto the surface of a four-dimensional sphere in $\vec{\rho}$ ($\vec{\pi}$) space, whose size depends on the energy. If the energy varies from $E=0$ to $E\to-\infty$, the entire $\vec{\rho}$ and $\vec{\pi}$ spaces are covered.

It should be noticed that in the transformation to $\vec{\rho}$ space, the Runge-Lenz vector appears as a parameter. This does not happen when transforming to $\vec{\pi}$ space. In consequence, it will be much simpler to shift from real to symmetrical space when dealing with momenta.

Transforming the equations of motion (1) to the symmetrical representation, we get

$$\frac{r}{r_E}\frac{d\rho_i}{dt} = \frac{\pi_i}{m}, \quad \frac{r}{r_E}\frac{d\pi_i}{dt} = -m\left(\frac{p_0}{mr_0}\right)^2\rho_i, \quad i=1,2,3.$$

These equations correspond to nonuniform circular motion. If we introduce the invariant time parameter

$$d\tau = \frac{r_E}{r}dt, \tag{10}$$

Hamilton equations read

$$\frac{d\rho_i}{d\tau} = \frac{\pi_i}{m}, \quad \frac{d\pi_i}{d\tau} = -m\left(\frac{p_E}{mr_E}\right)^2\rho_i, \quad i=1,2,3.$$

Thus, with these new spatial, momentum, and time variables, Kepler orbits appear as uniform circular motion along great circles [14] on a four-dimensional sphere. The angular velocity is $\omega = p_E/mr_E$.

Let us select a single orbit by fixing the values of $\mathbf{L}$ and $\mathbf{A}$. With them, L_E and E may be computed [Eq. (3)]. Writing $\mathbf{r}$ in terms of ρ_i, Eqs. (4) and (5) for the trajectory in coordinate space transform into a set of four linear homogeneous equations. In the same way as with relations (4) and (5), only two of them are independent. They can be written as

$$\begin{aligned}
0 &= \rho_1 v_1^a + \rho_2 v_2^a + \rho_3 v_3^a + \rho_4 v_4^a,\\
0 &= \rho_1 v_1^b + \rho_2 v_2^b + \rho_3 v_3^b + \rho_4 v_4^b,
\end{aligned} \tag{11}$$

where

$$\begin{pmatrix} v_1^a\\ v_2^a\\ v_3^a\\ v_4^a \end{pmatrix} = \frac{1}{L}\begin{pmatrix} L_1\\ L_2\\ L_3\\ 0 \end{pmatrix}, \quad \begin{pmatrix} v_1^b\\ v_2^b\\ v_3^b\\ v_4^b \end{pmatrix} = \frac{1}{LL_E}\begin{pmatrix} \mathbf{L}\times\mathbf{A}|_1\\ \mathbf{L}\times\mathbf{A}|_2\\ \mathbf{L}\times\mathbf{A}|_3\\ -L^2 \end{pmatrix}.$$

The system (11) defines a plane in $\vec{\rho}$ space, whose orientation depends on $\hat{L}$, $\hat{A}$, and α_0. The transformation (8) treats the energy (parametrized by r_E and L_E) as a variable. Therefore all the possible ellipses [Eqs. (4) and (5)] in $\mathbf{r}$ space that may be obtained by varying the energy are mapped into the plane defined by Eq. (11). To define a single trajectory, we have to fix the energy by including the constraint

$$r_0^2 = \rho_1^2+\rho_2^2+\rho_3^2+\rho_4^2. \tag{12}$$

So, the trajectory in $\vec{\rho}$ space is defined by the intersection of plane (11) with the hypersphere (12), giving a hypercircle of radius r_0.

In the same way, Eqs. (6) and (7) of the trajectory in momentum space transform into

$$\begin{aligned}
0 &= \pi_1 v_1^a + \pi_2 v_2^a + \pi_3 v_3^a + \pi_4 v_4^a,\\
0 &= \pi_1 v_1^b + \pi_2 v_2^b + \pi_3 v_3^b + \pi_4 v_4^b.
\end{aligned} \tag{13}$$

To this set of equations, the restriction

$$p_0^2 = \pi_1^2+\pi_2^2+\pi_3^2+\pi_4^2 \tag{14}$$

has to be added. Relations (13) and (14) define in $\vec{\pi}$ space the same hodograph as relations (11) and (12) in $\vec{\rho}$ space, except for the scale factor which is now given by p_0. When performing circular motion, a particle describes a circle with the same orientation in both coordinate and momentum space. There is, however, a phase shift of $\pi/2$ in the temporal variation of the particle on the two circles.

We see that Kepler trajectories turn out to be very simple in the symmetric representation. Both the ellipses in coordinate space and the circles in momentum space transform into geodesics of spheres in $\vec{\rho}$ and $\vec{\pi}$ space, as shown in Fig. 2. In

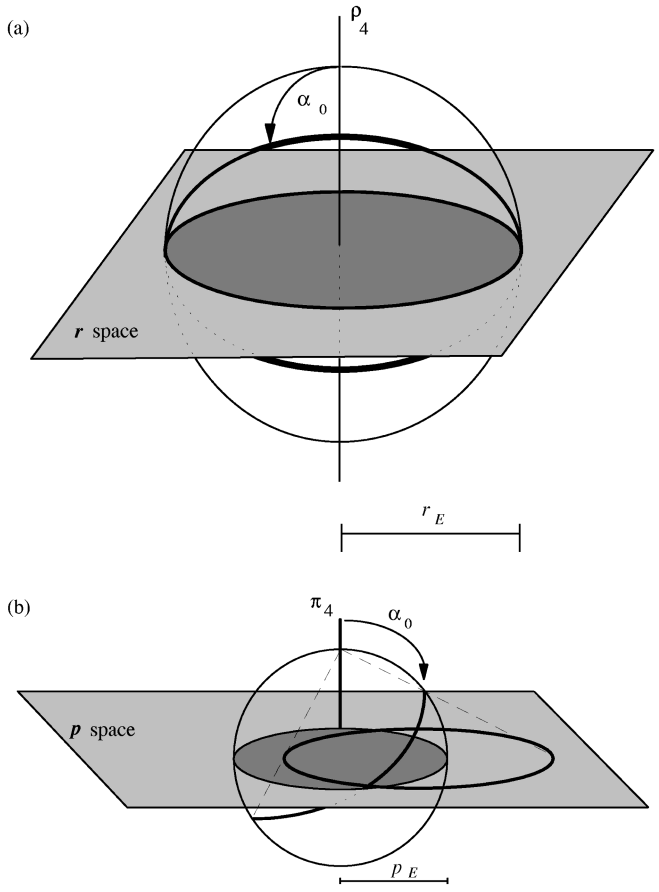

FIG. 2. (a) Parallel and (b) stereographic projections of an orbit (thick lines) in (a) coordinate and (b) momentum space to the corresponding spheres in (a) $\vec{\rho}$ and (b) $\vec{\pi}$ space. Real space has been drawn as a two-dimensional plane, in order to be able to include the fourth component of the new coordinates ρ_4 and π_4. In the symmetrical representation, Kepler orbits are geodesics which form an angle $\alpha_0=\arctan(L/A)$ with respect to the fourth axis $\hat{\rho}_4$ or $\hat{\pi}_4$.

symmetrical space, a given trajectory is tilted with respect to the axis $\hat{\rho}_4$ ($\hat{\pi}_4$) in the angle $\alpha_0=\arctan(L/A)$. Therefore, if $A=0$ and the orbits in real coordinate and momentum spaces are circular, the geodesics in the symmetric spaces are contained in the subspaces $\rho_4=0$ and $\pi_4=0$ and look the same as the real orbits. On the other hand, if $L=0$ and the trajectories in the real spaces degenerate into straight lines, in the symmetric representation they become upright circles, or meridians of the corresponding hyperspheres ($\hat{\rho}_4$ and $\hat{\pi}_4$ are directed towards the ''north pole'').

In what follows, it will be convenient to use polar coordinates in $\vec{\pi}$ space. We define

$$|\vec{\pi}|=\sqrt{\pi_1^2+\pi_2^2+\pi_3^2+\pi_4^2}, \quad \theta_P=\arctan\left(\frac{\sqrt{\pi_1^2+\pi_2^2}}{\pi_3}\right),$$

$$\alpha_P=\arctan\left(\frac{\sqrt{\pi_1^2+\pi_2^2+\pi_3^2}}{\pi_4}\right), \quad \varphi_P=\arctan\left(\frac{\pi_2}{\pi_1}\right).$$

The angles θ_P and φ_P are the usual polar angles in momentum space, and α_P is a function of p and p_E.

III. THE DENSITY IN MOMENTUM SPACE

We have seen that it is possible to map Kepler orbits onto uniform circular motion by means of a transformation which involves the coordinates of phase space, the energy, and a reparametrization of the temporal variable.

We now want to calculate a density in momentum space corresponding to an ensemble of classical orbits that simulates the quantum-mechanical Rydberg states. Such an ensemble has to be constructed with all the orbits in which E, L, and L_3 are fixed to certain values. There are many orbits which fulfill these conditions, and all of them should contribute to the density with equal probability. In symmetrical space all orbits have the same size, shape, and period. Furthermore, for a fixed energy, all trajectories correspond to the same uniform angular velocity. Therefore, when working with the symmetrical coordinates, the calculation of the density turns out to be straightforward. To obtain the particle distribution in momentum space we only need to make a coordinate transformation from the corresponding density in symmetrical space. Explicitly

$$\frac{dP}{d\mathbf{p}dp_E dt}=\left|\frac{\partial(\pi_1\pi_2\pi_3\pi_4\tau)}{\partial(p_1p_2p_3p_E t)}\right|\frac{dP}{d\pi d\tau}, \tag{15}$$

where dP is the probability of finding a particle about the position (π_1, π_2, π_3, π_4) at time τ, with a tolerance $(d\pi_1,d\pi_2,d\pi_3,d\pi_4)$ and $d\tau$ [or, similarly, about (p_1,p_2,p_3,p_E) at time t, in a volume (dp_1,dp_2,dp_3,dp_E) and dt]. The proportionality factor between the two distributions in Eq. (15) is the modulus of the Jacobian of the transformation between the variables $(\pi_1,\pi_2,\pi_3,\pi_4,\tau)$ and (p_1,p_2,p_3,p_E,t).

Using the coordinate transformation (8) and the time parametrization (10) the explicit calculation of the Jacobian can be carried out. The result is

$$\frac{\partial(\pi_1\pi_2\pi_3\pi_4\tau)}{\partial(p_1p_2p_3p_E t)}=\left(\frac{2p_E^2}{p_E^2+p^2}\right)^4=\left(\frac{2}{1+\sin^2\alpha_P}\right)^4. \tag{16}$$

A. Particle distribution for a single orbit

We begin calculating the distribution of particles in symmetrical space for a single orbit, when the initial position is uniformly distributed on the trajectory. To select an orbit, **L** and **A** have to be given specific values. Care has to be taken to fulfill Eq. (2). With these vectors, the energy is determined by Eq. (3). We define the parameters

$$p_0=\frac{mg}{\sqrt{(A^2+L^2)}}, \quad \alpha_0=\arctan(L/A).$$

Since the motion along the circle defined by Eqs. (13) and (14) is uniform, the density reads

$$\left.\frac{dP}{d\pi d\tau}\right|_{\mathbf{AL}}=\frac{1}{2\pi p_0}\delta(p_0-|\vec{\pi}|) \times\delta(\pi_1v_1^a+\pi_2v_2^a+\pi_3v_3^a+\pi_4v_4^a) \times\delta(\pi_1v_1^b+\pi_2v_2^b+\pi_3v_3^b+\pi_4v_4^b), \tag{17}$$

where the proportionality factor has been calculated by integrating in $\mathbf{p}$ and p_E and equating the result to unity. This normalization criterion will be employed throughout the paper. The distribution (17) is zero all over $\vec{\pi}$ space, except on the hypercircle defined by the selected values of $\mathbf{L}$ and $\mathbf{A}$. There, the three δ functions have vanishing arguments and the density diverges.

Using Eqs. (16) and (15) to transform back to momentum space, and after some algebraic manipulation, we obtain

$$\left.\frac{dP}{d\mathbf{p}dp_E dt}\right|_{\mathbf{AL}} = \frac{1}{2\pi p_0}\,\delta(p_E - p_0)\left(\frac{2p_E^2}{p_E^2+p^2}\right)^2 \frac{df^{\mathbf{AL}}}{d\mathbf{p}}(\mathbf{p}), \tag{18}$$

where

$$\frac{df^{\mathbf{AL}}}{d\mathbf{p}}(\mathbf{p}) = \delta(\mathbf{p}\cdot\hat{L})\,\delta\left\{\sqrt{[\mathbf{p}\cdot(\hat{A}\times\hat{L}) - p_0\cot\,\alpha_0]^2 + (\mathbf{p}\cdot\hat{A})^2} - \frac{p_0}{\sin\,\alpha_0}\right\}.$$

The distribution (18) is zero over all $\mathbf{p}$ space, except on the circle defined by $\mathbf{L}$ and $\mathbf{A}$ in Eqs. (6) and (7). The factor $df^{\mathbf{AL}}/d\mathbf{p}$ represents a uniform density per unit length on the orbit.

Let us analyze the origin of the factor $(2p_E^2/p_E^2+p^2)^2$. In momentum space, particles move along their orbits with a velocity $d\mathbf{p}/dt = -(g/r^2)\hat{r}$. Using energy conservation, we write $r \propto 1/(p^2+p_E^2)$. The probability per unit length of finding a particle in a specific position on its orbit is proportional to the inverse of its velocity in momentum space. In terms of p, this reads as $(2p_E/p^2+p_E^2)^2$.

B. Particle distribution for fixed L and *E*

We now calculate the distribution for an ensemble of trajectories, all corresponding to the same $\mathbf{L}$ and E, but with any $\mathbf{A}$. Since the constraints (2) and (3) must hold, $\mathbf{A}$ must be chosen perpendicular to $\mathbf{L}$ and with modulus equal to $\sqrt{L_E^2 - L^2}$. We construct our ensemble by selecting all those orbits which lie in the plane normal to $\mathbf{L}$, have an eccentricity $\epsilon = \sqrt{1 - L^2/L_E}$, and whose perihelion is oriented in any direction (see Fig. 3). Each of these trajectories gives a contribution to the density, of the type (18). We sum them all up, with equal probability,

$$\left.\frac{dP}{d\pi d\tau}\right|_{E\mathbf{L}} \propto \int_0^{2\pi} d\varphi_A \frac{dP}{d\pi d\tau}_{\mathbf{AL}}, \tag{19}$$

where φ_A is defined on the plane perpendicular to $\mathbf{L}$, and gives the orientation of vector $\mathbf{A}$. The (normalized) result of the integral in Eq. (19) is

$$\left.\frac{dP}{d\pi d\tau}\right|_{E\mathbf{L}} = \frac{1}{2\pi^2 p_0^2}\,\delta(\pi_1 v_1^a + \pi_2 v_2^a + \pi_3 v_3^a + \pi_4 v_4^a) \times \delta(|\pi| - p_0)\frac{\Theta(\cos^2\alpha_0 - \cos^2\alpha_P)}{\sqrt{\cos^2\alpha_0 - \cos^2\alpha_P}}, \tag{20}$$

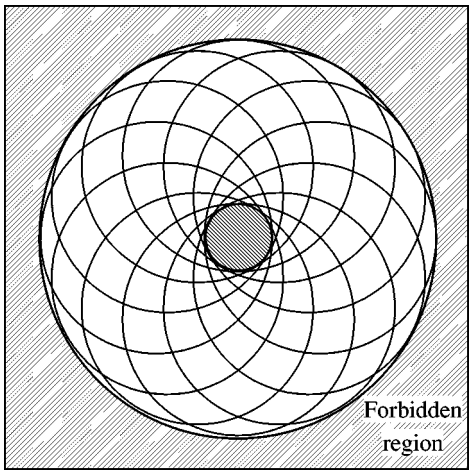

FIG. 3. Ensemble of trajectories in momentum space which contribute to the density for fixed $\mathbf{L}$ and E. The caustics are also shown.

where Θ stands for the Heaviside step function [15].

Transforming this distribution to momentum space through Eqs. (15) and (16), we get

$$\left.\frac{dP}{d\mathbf{p}dp_E t}\right|_{E\mathbf{L}} = \frac{1}{2\pi^2 p_0^2}\,\delta(\mathbf{p}\cdot\hat{L})\,\delta(p_E - p_0)\left(\frac{2}{1+p^2/p_E^2}\right)^3 \times \frac{\Theta[(p-p^-)(p^+-p)]}{\sqrt{\cos^2\alpha_0 - (p^2/p_E^2-1)^2/(p^2/p_E^2+1)^2}}, \tag{21}$$

where

$$p^{\pm} = p_E\frac{1 \pm \cos\,\alpha_0}{\sin\,\alpha_0}.$$

In Fig. 4 we show the factor accompanying the δ function in Eq. (21). There are divergencies at $p = p^{\pm}$. These are the

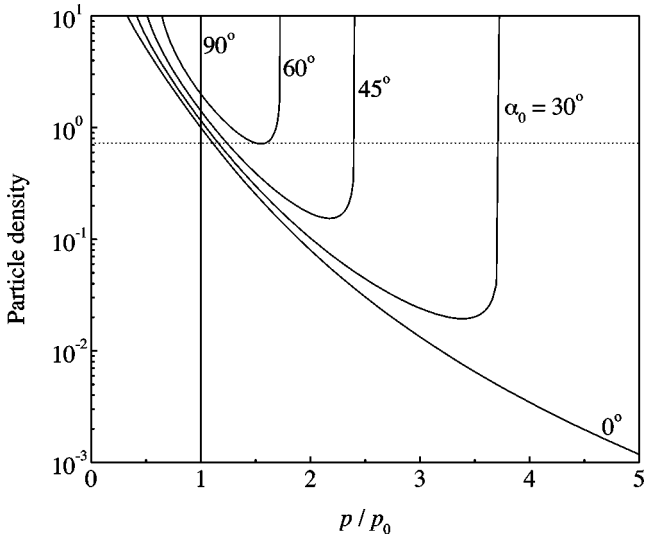

FIG. 4. Particle distribution in momentum space for fixed $\mathbf{L}$ and E, on the plane perpendicular to $\mathbf{L}$. We show the factor accompanying $\delta(\mathbf{p}\cdot\hat{L})$ for several values of $\alpha_0 = \arctan(L/A)$.

maximum and minimum values reached by the orbits in the ensemble. As shown in Fig. 3, at these two momenta trajectories accumulate to form caustics. For $p^- < p < p^+$ the particle distributions shows a smooth behavior. Outside this interval the density is strictly zero, since there are no particles reaching thus far. We see that as L increases, the range of the distribution becomes narrower. In fact, for $L = L_E$ ($\alpha_0 = 90°$), we only find particles with $p = p_E$. This corresponds to circular motion.

C. Particle distribution for L=0

The case of $\mathbf{L}=\mathbf{0}$ has to be treated separately. Clearly, it is not enough to take the limit $\alpha_0 \to 0$ in Eq. (21), since the term $\delta(\mathbf{p}\cdot\hat{L})$ restricts the orbits to a single plane. This plane has no meaning when $\mathbf{L}$ vanishes. Therefore, after making $\alpha_0 \to 0$, we must integrate over all the possible directions $\hat{L}$. The result is

$$\left.\frac{dP}{d\mathbf{p}dp_E dt}\right|_{E\mathbf{L}=\mathbf{0}} = \frac{1}{\pi^2 p_E^2}\,\frac{\delta(p_E - p_0)}{(p^2/p_E^2)(1+p^2/p_E^2)^2}. \qquad (22)$$

This distribution is spherically symmetrical. In fact, the trajectories which contribute to an ensemble with $\mathbf{L}=\mathbf{0}$ are ellipses that have degenerated into line segments in coordinate space, and into infinite straight lines in momentum space. The orbits that make up the ensemble are all the lines which pass through the origin. The distribution (22) diverges at the origin, and shows a smooth decrease for greater p. The divergency is related with the accumulation of trajectories at the origin. The decay as p^{-6} for large momenta comes from the particles that are at the far (infinite) end of the straight lines, where their momentum diverges.

D. Particle distribution for fixed E, L, and L_3

We now give a further step, allowing L_1 and L_2 to vary, while keeping L and L_3 fixed. In Fig. 5 we show the values of $\mathbf{L}$ that we have to consider. For each of these $\mathbf{L}$, there is a distribution of the form (21). In the same way as before, we construct the density by integrating our previous result.

Since fixing the value of L_3 implies the selection of a specific direction in space, we need to decompose

$$\mathbf{L} = L_E \sin\alpha_0(\cos\theta_L \hat{z} + \sin\theta_L \cos\varphi_L \hat{x} + \sin\theta_L \sin\varphi_L \hat{y}),$$

$$\mathbf{A} = L_E \cos\alpha_0(\cos\theta_A \hat{z} + \sin\theta_A \cos\varphi_A \hat{x} + \sin\theta_A \sin\varphi_A \hat{y}).$$

Using this notation in Eq. (20), we integrate

$$\left.\frac{dP}{d\pi d\tau}\right|_{ELL_3} \propto \int_0^{2\pi} d\varphi_L \left.\frac{dP}{d\pi d\tau}\right|^{E\mathbf{L}},$$

obtaining

$$\left.\frac{dP}{d\pi d\tau}\right|_{ELL_3} = \left(\frac{1}{2\pi^3 p_0^3}\right)\frac{\delta(|\vec{\pi}| - p_0)}{\sin\alpha_P} \times \frac{\Theta(\cos^2\alpha_0 - \cos^2\alpha_P)}{\sqrt{\cos^2\alpha_0 - \cos^2\alpha_P}}\,\frac{\Theta(\sin^2\theta_P - \cos^2\theta_L)}{\sqrt{\sin^2\theta_P - \cos^2\theta_L}}.$$

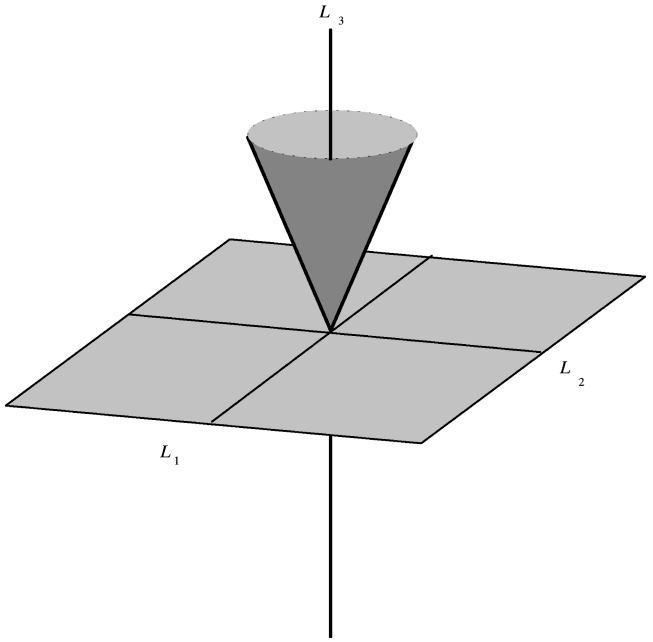

FIG. 5. The dotted line shows the angular momentum vectors which contribute to the density for fixed E, L^2, and L_3.

Transforming this distribution to $\mathbf{p}$ space, we get

$$\left.\frac{dP}{d\mathbf{p}dp_E d\tau}\right|_{ELL_3} = \frac{1}{2\pi^3 p_0^3}\,\delta(p_E - p_0)\frac{1}{p/p_E}\left[\frac{2}{1+(p/p_E)^2}\right]^3 \times \frac{\Theta[(p-p^-)(p^+-p)]}{\sqrt{[2pp_E/(p^2+p_E^2)]^2 - L^2/L_E^2}} \times \frac{\Theta[(\theta-\theta^-)(\theta^+-\theta)]}{\sqrt{\sin^2\theta_P - L_3^2/L^2}}, \qquad (23)$$

where

$$\theta_P^+ = \pi/2 + \theta_L, \quad \theta_P^- = \pi/2 - \theta_L \quad \text{if} \quad \theta_L < \pi/2,$$

$$\theta_P^+ = 3\pi/2 - \theta_L, \quad \theta_P^- = \theta_L - \pi/2 \quad \text{if} \quad \theta_L > \pi/2.$$

The distribution (23) is one of the main results of this paper, and is shown in Fig. 6 for particular values of α_0 and θ_L. We can see that, in addition to the divergency at $p_\pm$ of Eq. (21), there are two other caustics at $\theta = \theta^\pm$.

The greater the value of L_3/L, the more sharply defined is the angular momentum. Therefore as we increase $\cos\theta_L$ the distribution (23) tends to be confined to the plane spanned by p_1 and p_2.

E. Conserved quantities with continuous variation

Up to now we have considered the conserved quantities as having fixed definite values. This is analogous to what happens in the quantum-mechanical Rydberg states. A wave function with quantum numbers n, ℓ, and m has unit probability of bearing an energy $E = -mg^2/2\hbar^2 n^2$, a squared angular momentum $L^2 = \hbar^2 \ell(\ell+1)$, and its $\hat{z}$ component $L_3 = \hbar m$. To cover all the possible angular momenta, we have to consider the discrete set of pairs (ℓ, m), with ℓ

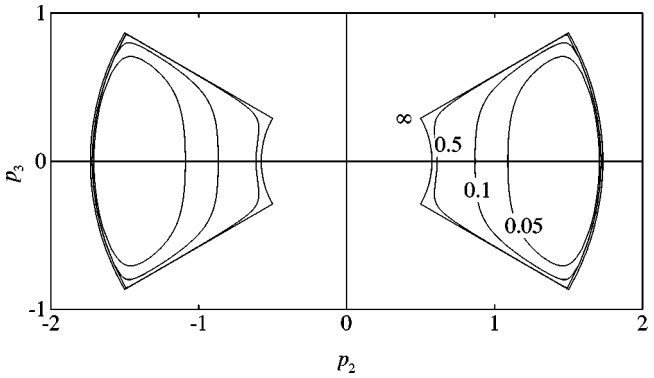

FIG. 6. Contour plot of the particle distribution for fixed E, L, and L_3, for $L=L_E\sin 60°$ and $L_3=L\cos 30°$. The density is depicted in the plane spanned by p_2 and p_3, and it has rotation symmetry about the axis p_3. There are divergencies at $p=p^{\pm}$ and at $\theta=\theta^{\pm}$ (see text).

$=0,1,\ldots,n-1$ and $m=-\ell,-\ell+1,\ldots,\ell$. This is in contrast to what happens in the classical description, where all the possible angular momenta are obtained by a continuous variation of L and L_3. As a matter of fact, the distributions calculated in the previous sections may be evaluated for any real value of the parameters $L\in[0,L_E]$, and $L_3\in[-L,L]$. This discrepancy between the two approaches raises the question of whether assigning a fixed value for L and L_3 is a good classical description of the quantum-mechanical situation. Instead, the classical description of a Rydberg state can be constructed with an ensemble of trajectories which have L and L_3 not with definite values, but belonging to a small interval. The possible intervals for L are the result of partitioning the segment $[0,L_E]$ in n equal portions. Correspondingly, the intervals for L_3 come from the division of $[-L,L]$ in $2\ell+1$ ribs. In this description we will no longer have classical distributions with fixed values of L^2 and L_3. But, in compensation, we will construct distributions that cover a nonvanishing portion of the allowed parameter space, just as it happens in quantum mechanics. In the present section we follow this approach.

We want to describe a state with quantum numbers n, ℓ, and m. Since in the classical approach $L_E^2=-g^2m/2E$, and quantum mechanics states that $E=-mg^2/2\hbar^2n^2$, we associate

$$L_E=\hbar n. \tag{24}$$

The classical available interval for L is $[0,L_E]$. If we divide it in n portions, each subinterval is $\hbar$ wide. The one corresponding to the state (n,ℓ,m) begins at $\hbar\ell$ and ends at $\hbar(\ell+1)$. Correspondingly, in the classical description, L_3 can have any value belonging to $[-L,L]$. Dividing this interval in $2\ell+1$ pieces, each rib has a width of $2L/(2\ell+1)$. Consequently, our state gets $L_3\in[L(2m-1)/(2\ell+1),L(2m+1)/(2\ell+1)]$.

As a first step, then, we allow L_3 to vary in its rib with uniform probability. Once more, we construct our distribution by integrating our previous result. Writing $L_3=L\cos\theta_L$, we have

$$\left.\frac{dP}{d\pi d\tau}\right|_{EL[\theta_L^i,\theta_L^f]}\propto L\int_{\theta_L^i}^{\theta_L^f}\sin\theta_L\ d\theta_L\frac{dP}{d\pi d\tau}^{EL\,L\cos\theta_L}, \tag{25}$$

where

$$\theta_L^i=\arccos\left[\frac{2m+1}{2\ell+1}\right],\quad \theta_L^f=\arccos\left[\frac{2m-1}{2\ell+1}\right]. \tag{26}$$

In Eq. (25) the subindex $[\theta_L^i,\theta_L^f]$ in the left hand side means that L_3 belongs to the interval $[L\cos\theta_L^f, L\cos\theta_L^i]$.

The following step consists in allowing the variation of L in $[L^i,L^f]$. Thus

$$\left.\frac{dP}{d\pi d\tau}\right|_{E[L^i,L^f][\theta_L^i,\theta_L^f]}\propto\int_{L^i}^{L^f}dL\frac{dP}{d\pi d\tau}^{EL[\theta_L^i,\theta_L^f]}, \tag{27}$$

where the subindex $[L^i,L^f]$ indicates that $L\in[L^i,L^f]$ with uniform distribution. In relation to the state with quantum numbers (n,ℓ,m),

$$L^i=\hbar\ell,\quad L^f=\hbar(\ell+1). \tag{28}$$

The normalized result of the integration of Eqs. (27) and (25) is

$$\begin{aligned}\left.\frac{dP}{d\pi d\tau}\right|_{E[L^i,L^f][\theta_L^i,\theta_L^f]}=&\frac{1}{2\pi^3p_0^3}\frac{1}{\cos\beta^f-\cos\beta^i}\\&\times\frac{2L_E^2}{(L^f)^2-(L^i)^2}\frac{\delta(|\pi|-p_0)}{\sin\alpha_P}\\&\times[\arcsin\beta^i-\arcsin\beta^f]\\&\times[\sqrt{\cos^2\gamma^i-\cos^2\alpha_p}\\&-\sqrt{\cos^2(\gamma^f)-\cos^2(\alpha_P)}],\end{aligned} \tag{29}$$

where

$$\beta^{i,f}=S\left(\frac{\cos\theta_L^{i,f}}{\sin\theta_P}\right),$$

and

$$S(x)=\begin{cases}-1 & \text{if}\quad x<-1\\ x & \text{if}\quad |x|<1\\ 1 & \text{if}\quad x>1\end{cases}$$

and

$$\cos^2\gamma^{i,f}=\max[\cos^2\alpha_P,1-(L^{i,f}/L_E)^2].$$

The transformation of Eq. (29) to **p** space is straightforward, using Eqs. (8), (15), and (16). The distribution thus obtained may be separated in two factors, one depending on p and p_E, and the other on θ_P and φ_P. Explicitly

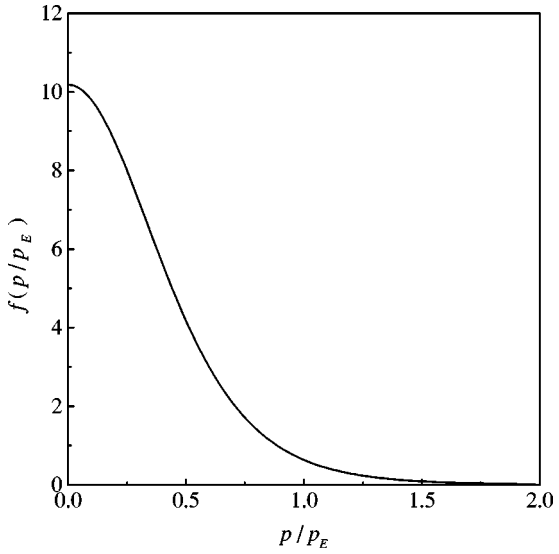

FIG. 7. Microcanonical distribution found both in the classical and the quantum-mechanical description, when all states with fixed energy are considered with equal probability.

$$\left.\frac{dP}{d\mathbf{p}dp_E dt}\right|_{E[L^i,L^f][\theta_L^i,\theta_L^f]} = f^C_{E,[L^i,L^f]}(p,p_E)\, g^C_{[\theta_L^i,\theta_L^f]}(\theta_P,\varphi_P), \tag{30}$$

with

$$f^C_{E,[L^i,L^f]}(p,pE) = \frac{2}{\pi p_0^3}\quad \frac{L_E^2}{(L^f)^2-(L^i)^2}\,\delta(p_E-p_0) \times \frac{p_E^2+p^2}{2pp_E}\left(\frac{2p_E^2}{p^2+p_E^2}\right)^4 \times\left[\sqrt{\cos^2\gamma^i-\cos^2[(p_0^2-p^2)/(p_0^2+p^2)]}\right. - \left.\sqrt{\cos^2\gamma^f-\cos^2[(p_0^2-p^2)/(p_0^2+p^2)]}\right],$$

$$g^C_{[\theta_L^i,\theta_L^f]}(\theta_P,\varphi_P) = \frac{1}{2\pi^2}\,\frac{1}{\cos\,\theta_L^f-\cos\,\theta_L^i} \times[\arcsin\,\beta^i-\arcsin\,\beta^f]. \tag{31}$$

Equations (30) and (31) are the other important result of this paper. What remains of this section is dedicated to studying some of their properties, and to the comparison with their quantum-mechanical analog. In this comparison, the parameters of Eqs. (31) have to be taken from Eqs. (24), (26), and (28).

In the first place, when we make the width of the ribs in L and L_3 tend to zero, the distribution (30) goes to Eq. (23). On the other hand, if we take the ribs as wide as possible ($L^i=0, L^f=L_E, \theta_L^i=0, \theta_L^f=\pi$), we obtain the microcanonical density

$$\left.\frac{dP}{d\mathbf{p}dp_E dt}\right|_E = \frac{1}{2\pi^2 p_E^3}\,\delta(p_E-p_0)\left(\frac{2p_E^2}{p^2+p_E^2}\right)^4, \tag{32}$$

shown in Fig. 7. This distribution was derived by Pitaevskii [16], Omidvar [17], Mapleton [18], and Abrines and Percival [19]. It happens to be exactly equal to the corresponding quantum-mechanical density, derived by Fock [13]. This identity between the classical and quantum-mechanical descriptions of the microcanonical distribution constitutes one of the complete correspondence identities of the Coulomb potential. It has been extensively studied by Norcliffe and Percival [20].

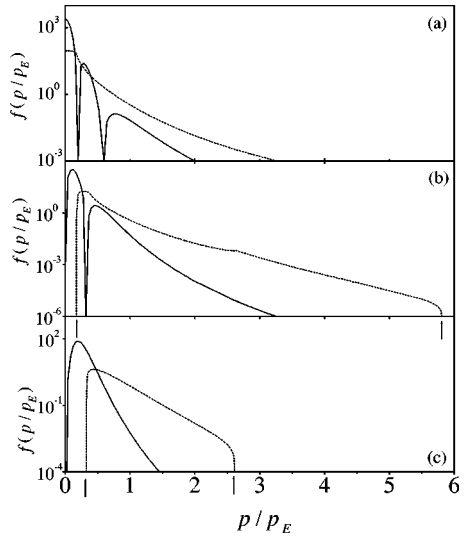

FIG. 8. Comparison between the classical f^C (dotted line) and the quantum-mechanical f^Q (full line) radial Rydberg momentum distributions, corresponding to $n=3$. (a) $f^C_{[0,L_E/3]}$ and $f^Q_{n=3,\ell=0}$, (b) $f^C_{[L_E/3,2L_E/3]}$ and $f^Q_{n=3,\ell=1}$, (c) $f^C_{[2L_E/3,L_E]}$ and $f^Q_{n=3,\ell=2}$. The values of $p_{\min}$ and $p_{\max}$ are indicated by arrows, in (b) and (c). At these momenta, the derivatives of (a) and (b) show discontinuities.

A factorization of the type (30) can also be done with the quantum distributions, namely,

$$\left.\frac{dP}{d\mathbf{p}dp_E dt}\right|_{n,\ell,m} = f^Q_{n,\ell}(p,p_E)\, g^Q_{\ell,m}(\theta_P,\varphi_P),$$

with

$$f^Q_{n,\ell}(p) = \left|\sqrt{\frac{2(n-\ell-1)!}{\pi(n+1)!}}\,2^{2\ell+2}\ell!\,n^2\,\frac{(np/p^*)^\ell}{[(np/p^*)^2+1]^{\ell+2}} \times \mathcal{C}^{\ell+1}_{n-\ell-1}\left[\frac{(np/p^*)^2-1}{(np/p^*)^2+1}\right]\right|^2,$$

$$g^Q_{\ell,m}(\theta_P,\varphi_P) = |\mathcal{Y}^m_\ell(\theta_P,\varphi_P)|^2. \tag{33}$$

Here, $p^*=mg/\hbar$ is the mean value of the momentum in the ground state. The symbol $\mathcal{C}$ represents a Gegenbauer function, and $\mathcal{Y}$ stands for a spherical harmonic [21]. The dependence of $\mathcal{Y}$ upon the azimuthal angle φ_P is only through a phase, and it disappears when taking the square modulus.

The quantization of n brings about a quantization of the energy, and hence, of p_E. Since $n=p^*/p_E$, we may write f^Q as a function of p/p_E alone, just as it happens in the classical description, Eq. (31).

In Fig. 8 we compare f^C and f^Q, for $n=3$. There are three quantum-mechanical distributions, corresponding to ℓ

$=0$, 1, and 2. The classical analogs have L uniformly distributed in three intervals $[0,L_E/3]$, $[L_E/3,2L_E/3]$, and $[2L_E/3,L_E]$. If we sum up the three quantum mechanical distributions and normalize, we get the microcanonical density of Eq. (32). We have proved that this also happens when the three classical densities are added together.

Except for the case of $\mathbf{L}=\mathbf{0}$, classical trajectories are bounded. In consequence, the corresponding densities begin and end abruptly. The first and last momenta for which f^C is different from zero are

$$p_{\min}=p_E \tan 2\alpha_0^i, \quad p_{\max}=p_E \cot 2\alpha_0^i,$$

where $\alpha_0^i=\arcsin(L^i/L_E)$. In contrast, the distribution that contains $\mathbf{L}=\mathbf{0}$ ($L^i=0$) ranges from $p=0$ to $p=\infty$, as happens with the microcanonical density (32). In fact, for small and large momenta, these two distributions coincide exactly. $f^C|_{E[0,\alpha_0^f]}$ differs from $dP/dp|_E$ in a finite interval $(p_E\tan 2\alpha_0^f, p_E\cot 2\alpha_0^f)$, where the other two distributions are different from zero. In terms of the participating trajectories, the smaller the angular momentum, the larger the spectrum of values of p. If $\mathbf{L}=\mathbf{0}$, the orbit contains momenta which range from $p=0$ to $p=\infty$. On the other hand, for $L=L_E$ there is a single value for p, namely, p_E.

In Fig. 8 we see that the quantum-mechanical distribution also exhibits a sharper spectrum for large ℓ than for $\ell=0$. In this case, however, distributions do not end up abruptly, nor do they have discontinuous derivatives.

We now turn to the angular behavior of the classical and the quantum-mechanical densities. In Fig. 9, we compare g^C and g^Q. We see that when L_3 is large, the particle is confined to $\theta_P\approx\pi/2$. As m becomes smaller, the former maximum is split in two new ones, one of them shifted to lower angles and the other to larger angles. In the classical picture, for all $L_3<L$ there are no trajectories entirely contained in the plane normal to $\hat{p}_z$. Therefore if we diminish L_3 a minimum begins to show near $\pi/2$. As $L_3\approx 0$, the angular momentum vector lies in the (p_x,p_y) plane. The corresponding orbits are aligned with $\hat{p}_z$, confining the probability distribution to angles 0 and π.

We have proved that the relations

$$g_{\ell,-m}(\theta_P,\varphi_P)=g_{\ell,m}(\theta_P,\varphi_P),$$

$$\sum_{m=-\ell}^{\ell} g_{\ell,m}(\theta_P,\varphi_P)=\frac{2\ell+1}{4\pi}=\text{const}$$

hold, both for the classical and the quantum-mechanical angular distributions [to get the classical parameters, Eqs. (24), (26), and (28) should be used].

We have depicted the distributions f for $n=3$ and g for $\ell=2$. When these numbers increase, the classical and the quantum-mechanical densities approach each other.

IV. THE DENSITY IN COORDINATE SPACE

As we have mentioned earlier, the transformation (8) from coordinate space to symmetric variables bears a parametric dependence on $\mathbf{A}$. This means that the transformation itself depends on the orbit we are working on. Unless additional specifications are made, in general it is not possible to calculate the Jacobian of the transformation analytically, as in Eq. (16).

Here, we show briefly an example which comes out analytically, namely, the case of fixed energy and $\mathbf{L}=\mathbf{0}$. In coordinate space, this situation corresponds to ellipses which have degenerated into lines. In the symmetrical representation the orbits appear as meridians, when $\hat{\rho}_4$ is taken to point towards the north pole. Such ensemble of orbits gives rise to a distribution

$$\left.\frac{dP}{d\rho d\tau}\right|_{E\mathbf{L}=\mathbf{0}}=\lambda\,\delta(|\vec{\rho}|-r_0)\frac{|\vec{\rho}|^2}{\rho_1^2+\rho_2^2+\rho_3^2},$$

where $E=-g/2r_0$. The Runge-Lenz vector is, in this case,

$$\mathbf{A}=-p_E r_E\frac{\mathbf{r}}{r}=-L_E\hat{r}.$$

With this relation we calculate the Jacobian of the transformation (8). We get

$$\left|\frac{\partial(\pi_1\pi_2\pi_3\pi_4\tau)}{\partial(r_1r_2r_3r_Et)}\right|=\frac{1}{r_E^3}\frac{(r/r_E-1)^2}{(r/r_E)^{3/2}\sqrt{2-r/r_E}}.$$

Thus our (normalized) distribution reads

$$\left.\frac{dP}{d\mathbf{r}dr_Edt}\right|_{E\mathbf{L}=\mathbf{0}}=\frac{\delta(r_E-r_0)}{4\pi^2r_E^3}\frac{\Theta(2-r/r_E)}{(r/r_E)^{3/2}\sqrt{2-r/r_E}}.$$

This density diverges at the two turning points of the trajectories, that is, at $r=0$ and $r=2r_E$. The situation is spherically symmetrical, so the distribution depends only on r.

V. CONCLUSIONS

We have presented a method for calculating the particle distribution in momentum space for Rydberg states. The results allowed us to interpret some of the characteristics of the quantal distribution, in terms of the corresponding classical trajectories.

The main idea involved the selection of the classical trajectories which fulfill certain conditions imposed upon their constants of motion, in order to represent Rydberg states. We calculated the total density by summing up the individual densities of the participating trajectories. The method bears an important discrepancy with the quantum-mechanical approach, where only amplitudes can be added together. In the semiclassical limit of quantum mechanics, stationary states are calculated as a sum of individual amplitudes corresponding to classical trajectories [22]. The square modulus of each amplitude is equal to the probability of having such an orbit. However, each term has also a phase factor, which gives rise to path interference, and the corresponding oscillatory distributions (see Figs. 8 and 9). The classical result is obtained when the wavelength of the oscillations tends to zero.

Oscillations are not the only difference between the classical and the quantum-mechanical approaches. Classical distributions often show shadow zones, due to the fact that conservation laws forbid the presence of particles in certain regions (see Fig. 3). In the corresponding quantal descrip-

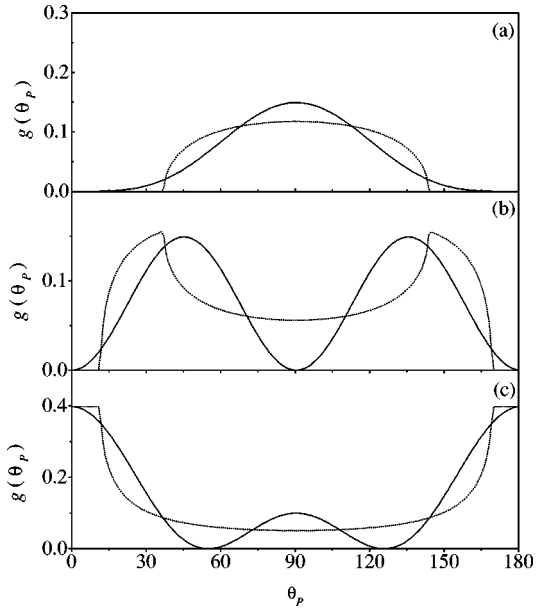

FIG. 9. Comparison between the classical g^C and the quantum-mechanical g^Q angular Rydberg momentum distributions, corresponding to $\ell=2$. (a) $g^C_{[\arccos(1),\arccos(3/5)]}$ and $g^Q_{\ell=2,m=2}$, (b) $g^C_{[\arccos(3/5),\arccos(1/5)]}$ and $g^Q_{\ell=2,m=1}$, (c) $g^C_{[\arccos(1/5),\arccos(-1/5)]}$ and $g^Q_{\ell=2,m=0}$.

tion, the probability of finding a particle in such regions is small, but not zero. We then talk about diffraction into the geometrical shadow, making an analogy with optics. In the semiclassical description, these zones are reached by some ghost trajectories [22] whose probability tends to zero in the classical limit.

Could we use our method for calculating classical distributions in some other system? In a general situation, a classical trajectory is identified by the value of its initial position and momentum. The Coulomb problem is an integrable one. In consequence, its orbits may also be labeled by the values of the constants of motion. In other words, picking up specific values for all the conserved quantities is equivalent to selecting a single orbit. We may then establish a one-to-one correspondence between the set of all the possible values of the constants of motion and all the possible trajectories. Therefore, in order to define a probability distribution on a set of orbits, it is sufficient to give the corresponding distribution for its constants of motion. We borrow such distribution from quantum mechanics. When the conserved quantities of a problem are known, there is a basis of stationary states that are also eigenstates of a set of selected commuting operators. Rydberg states, for example, are eigenfunctions of the Hamiltonian, the square of the angular momentum, and one of its components. The magnitudes corresponding to the commuting operators have definite values, while all the other independent conserved quantities are completely blurred. This defines the distribution of the constants of motion. Classically, this distribution can be expressed in terms of a distribution of trajectories, and hence, a distribution in coordinate and momentum spaces. In conclusion, the approach is valid whenever there is an integrable problem and there is a distribution for the conserved quantities. Such a distribution appears naturally from the geometry of the system under study. For example, a collision process favors the description in terms of parabolic coordinates and imposes a homogeneous distribution for L, since all impact parameters should appear with equal probability.

ACKNOWLEDGMENTS

This work has been supported by Consejo Nacional de Investigaciones Científicas y Técnicas. Enlightening discussions with R. O. Barrachina, W. Pregliasco, and J. Fiol are gratefully acknowledged. The author also thanks D. Zanette for his critical reading of the manuscript.

[1] J. Hare, M. Gross, and P. Goy, Phys. Rev. Lett. **61**, 1938 (1988).
[2] S. B. Hansen, T. Ehrenreich, E. Horsdal-Pedersen, K. B. MacAdam, and L. J. Dubé, Phys. Rev. Lett. **71**, 1522 (1993).
[3] J. C. Day, T. Ehrenreich, S. B. Hansen, E. Horsdal-Pedersen, K. S. Mogensen, and K. Taulbjerg, Phys. Rev. Lett. **72**, 1612 (1994).
[4] T. Ehrenreich, J. C. Day, S. B. Hansen, E. Horsdal-Pedersen, K. B. MacAdam, and K. S. Mogensen, J. Phys. B **27**, L383 (1994).
[5] K. S. Mogensen, J. C. Day, T. Ehrenreich, E. Horsdal-Pedersen, and K. Taulbjerg, Phys. Rev. A **51**, 4038 (1995).
[6] I. C. Percival and D. Richards, Adv. At. Mol. Phys. **11**, 1 (1975).
[7] M. Macholm, E. Lewartowski, and C. Courbin, J. Phys. B **27**, 4703 (1994).
[8] M. Macholm, E. Lewartowski, and C. Courbin, J. Phys. B **27**, 4681 (1994).
[9] J. Wang and R. E. Olson, Phys. Rev. Lett. **72**, 332 (1994).
[10] J. Wang and R. E. Olson, J. Phys. B **27**, 3707 (1994).
[11] D. M. Homan, M. J. Cavagnero, and D. A. Harmin, Phys. Rev. A **51**, 2075 (1995).
[12] G. Györgyi, Nuovo Cimento A **53**, 717 (1968).
[13] V. Fock, Z. Phys. **98**, 145 (1936).
[14] We use the expressions *great circle*, *geodesic*, and *hodograph* on a sphere of three or more dimensions, as a circle on the surface of the sphere with the same radius as the sphere.
[15] $\Theta(x)=1$ if $x>0$, and $\Theta(x)=0$ if $x\leqslant 0$.
[16] L. P. Pitaevskii, Zh. Éksp. Teor. Fiz. **42**, 1326 (1962) [Sov. Phys. JETP **15**, 919 (1962)].
[17] K. Omidvar, Goddard Space Flight Center Report No. X-641-65-306, 1965.
[18] R. A. Mapleton, Proc. Phys. Soc. London **87**, 219 (1966).
[19] R. Abrines and I. C. Percival, Proc. Phys. Soc. London **88**, 861 (1966).
[20] A. Norcliffe and I. C. Percival, J. Phys. B **1**, 784 (1968).
[21] I. S. Gradshteyn and I. M. Ryzhik, *Table of Integrals, Series and Products* (Academic Press Inc., New York, 1994).
[22] M. V. Berry and K. E. Mount, Rep. Prog. Phys. **35**, 315 (1972).